The Astrophysical Journal, 827:87 (11pp), 2016 August 10 doi:10.3847/0004-637X/827/1/87

A BUTTERFLY DIAGRAM AND CARRINGTON MAPS FOR CENTURY-LONG Ca II K SPECTROHELIOGRAMS FROM THE KODAIKANAL OBSERVATORY

Subhamoy Chatterjee[1], Dipankar Banerjee[1,2], and B. Ravindra[1]
[1] Indian Institute of Astrophysics, Koramangala, Bangalore 560034, India; dipu@iiap.res.in
[2] Center of Excellence in Space Sciences India, IISER Kolkata, Mohanpur 741246, West Bengal, India
Received 2016 April 1; revised 2016 May 23; accepted 2016 May 24; published 2016 August 10

ABSTRACT

The century-long (1907–2007) Ca II K spectroheliograms from the Kodaikanal Solar Observatory (KSO) are calibrated, processed, and analyzed to follow the evolution of the bright on-disc structures called plages, possible representatives of magnetic activity on the Sun. This is the longest data set studied in Ca II K to date, covering about 9.5 cycles of 11 yr periods. Plages are segmented with area $\geqslant 1$ arcmin^2 using global thresholds for individual full disc images and subsequent application of a morphological closing operation. The plage index is calculated and is seen to have a close positive correlation with the fractional disc area covered by plages. The newly generated plage area cycle (from KSO) was compared with the same from the Mount Wilson Observatory (correlation 95.6%) for the overlapping years, i.e., 1915–2000. This study illustrates the time–latitude distribution of plage centroids by rendering a butterfly diagram (as observed for sunspots). The 3D visualization of the diagram shows one-to-one mapping between plage location, time, and area. This work further delineates the positional correlation between magnetic patches and plage regions through the comparison of synoptic maps derived from both KSO Ca II K images and space-based full disc line-of-sight magnetograms. Regular synoptic magnetograms from ground-based observatories are available only after 1970s. Thus the long term Ca II K data from KSO can be used as a proxy for estimating magnetic activity locations and their strengths at earlier times.

Key words: astronomical databases: miscellaneous – methods: data analysis – Sun: chromosphere – Sun: faculae, plages – Sun: magnetic fields – techniques: image processing

Supporting material: animations

1. INTRODUCTION

Astronomical objects like stars are embedded with self-organizing system behavior which is expressed in different scales and modes over time. Multimodal long-duration data may assist in gaining insight about such complex system dynamics. As we are part of the solar system it is of particular interest for us to study the evolution of spatially resolved features on the Sun. In this regard, long term data available from different ground-based observatories provide valuable information at different wavelengths. Ca II K (3933.67 Å), the line of singly ionized calcium, is one such study wavelength. This absorption line extends our knowledge of the solar chromosphere (Stix 2004). The intensities observed in this line are dependent on the magnetic field strength. The locations of higher magnetic fields are correlated with bright regions in Ca II K solar intensity images (Harvey & Worden 1998; Sheeley et al. 2011). Thus Ca II K line emission provides a good proxy for line-of-sight (LOS) magnetic field fluxes, particularly for the historical period for which regular direct magnetic field measurements are not available (Skumanich et al. 1975; Schrijver et al. 1989). The Kodaikanal Solar Observatory (KSO) has archived full disc Ca II K spectroheliograms for more than a century (1906 to mid-2007), using photographic plates as recorded through a telescope with a 30 cm objective, with an *f*-ratio of $f/21$ (Priyal et al. 2014b). The effective spatial resolution was about 2 arcsec for the majority of the documentation time. Recently, 16 bit digitization has been performed for these plates using a CCD sensor (pixel size 15 μm cooled at -100°C) to generate 4096×4096 raw images. These data provide a significant temporal window (Foukal et al. 2009) to study the evolution of solar activity while studying the variation of disc structures, namely plages, filaments, and sunspots (Zharkova et al. 2005). Comparing the quality of different Ca II K images as recorded from the Arcetri Observatory, KSO, and the Mount Wilson Observatory (MWO), Ermolli et al. (2009) concluded that KSO provides a homogeneous series and is also the longest. Note that this comparison was made based on earlier low resolution scanned images (as obtained from KSO) and the need for higher resolution digitization was pointed out by Ermolli et al. (2009). The first results from the new digitization process were reported in Priyal et al. (2014b) using KSO data on Ca II K for the period 1955–1985. We have recalibrated the data for the full 100 years and are presenting the first results from the new time series. The data extracted through this study are also being made available to the scientific community for further processing. The digitized data are available through https://kso.iiap.res.in/data.

A few previous studies have reported the identification of chromospheric features and the generation of time series to understand the long term variation of their sizes and locations. However, none of these studies used century-long data, which allows us to study several solar cycles and inter-cycle variation, and this may help our understanding of the the solar dynamo model (Jin & Wang 2015). In the context of data processing, detection methods typically rely on the intensity contrast and the size of the target features. However, the contrast may differ between images, causing mis-detection of structures. Also, such techniques suffer from the fragmentation of segmented features, resulting in centroid detection errors (Zharkova et al. 2005). In the present work, we used newly digitized higher resolution century-long KSO Ca II K data for automated plage detection. This generated a number of time series (namely an area cycle,

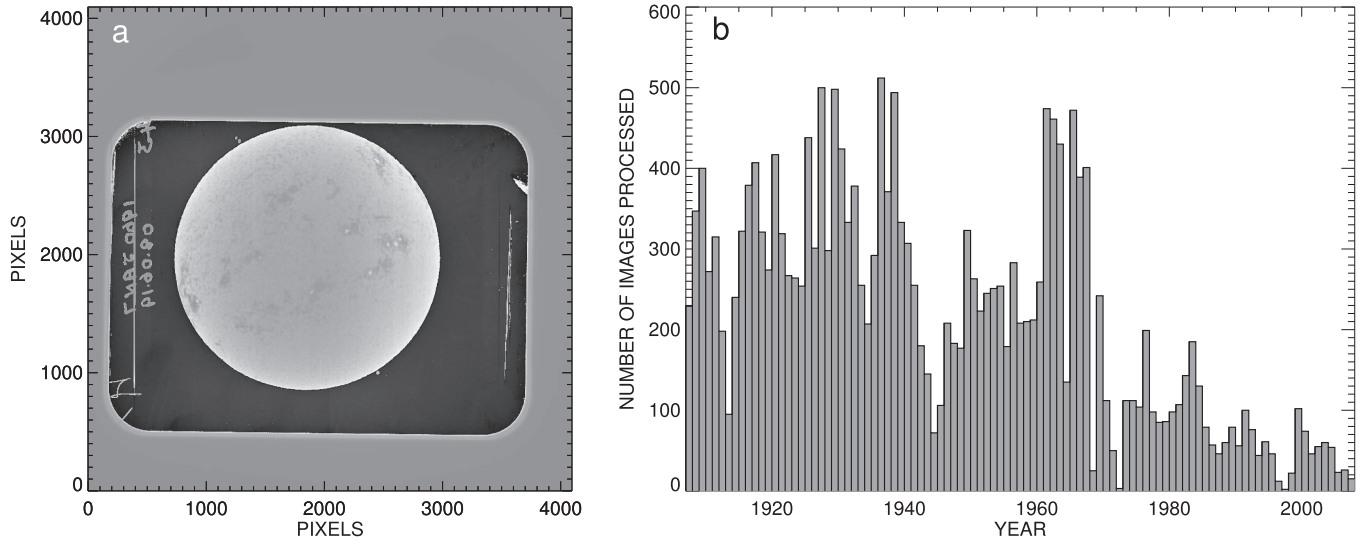

Figure 1. Input for the processing. (a) One representative Ca II K spectroheliogram raw image from KSO; (b) Ca II K image histogram showing the number of images considered for processing for each year.

butterfly diagram, and their combination) to facilitate the study of solar activity variation, keeping in mind the limitations and constraints. Section 2 illustrates the image statistics, calibration, enhancement, and processing techniques. The method to generate synoptic Carrington rotation (CR) maps from the data is also explained in this section. Section 3 describes the plage area cycle, butterfly diagram, and positional correlation of some Ca II K CR maps with the same generated from LOS magnetograms. The CR maps corresponding to the 100 yr are available online. We discuss the relevance of our results and present our conclusions in Section 4.

2. METHODS

The digitized full disc century-long (1907 to mid-2007) 4096 × 4096 Ca II K solar images (≈0.8036 arcsec pixel^{-1}) from KSO (Figures 1(a)–(b)) used in this study were recorded through a telescope with a 30 cm objective, with an f-ratio of $f/21$ (Priyal et al. 2014b) and a spatial resolution of about 2 arcsec. We employed a few calibration steps before the feature detection was performed: flat fielding, disc detection and centering, north–south rotation correction, intensity inversion, and limb darkening correction. The Hough circle transform (Sonka et al. 2014) was applied on the edge detected raw images to efficiently identify the disc center and radius, in contrast to the manual method described in earlier work by Priyal et al. (2014b). The radius varied by some number of pixels systematically over time due to a change in the Sun–Earth distance during each revolution. All the disc centered images were rescaled to one fixed size ($N \times N$) with a uniform disc radius (R) (Figure 2(a)).

2.1. Limb Darkening Correction

Limb darkening is a systematic large scale variation of solar intensity from center to limb due to the LOS effect. This should ideally be a radially symmetric function, but due to atmospheric and instrumental effects it loses the symmetry. In contrast to the radially symmetric polynomial method of limb darkening estimation for KSO data as presented in Priyal et al. (2014b), the current study captured the variation by applying a 40 × 40 2D median filter (Zharkova et al. 2005; Bertello et al. 2010) on the resized 512 × 512 disc centered images. This essentially performs blurring to represent large scale intensity variation (Figures 2(b)–(c)). Subsequently, the filtered image was again resized to the original 4096 × 4096 size and was used to correct for limb darkening in the original image (Figure 2(d)).

2.2. Plage Detection

Histogram equalization was applied on the limb darkening corrected images (LDC) to bring uniformity in intensity contrast throughout the study time and to enhance the target features with respect to the background. There was no absolute intensity calibration or full disc flux measurement (Foukal & Lean 1988), unlike in Ermolli et al. (2009). The objective was only to detect plages. Global thresholds were then applied on the histogram equalized images to generate binary images (BW) with segmented regions of interest. Enhanced limb darkening corrected images were characterized by the disc region intensity median ($\text{median}_{\text{Disc}}$) and standard deviation (σ_{Disc}). The disc region was described by pixels (i, j) satisfying $\sqrt{\left(i-\frac{N}{2}\right)^2+\left(j-\frac{N}{2}\right)^2} \leqslant R$. The segmentation scheme was as follows:

$$\begin{aligned} \text{BW}_{ij} &= 1 \text{ when } \text{LDC}^{\text{HistEqual}}{}_{ij} > \text{median}_{\text{Disc}} + \sigma_{\text{Disc}} \\ &= 0 \text{ otherwise.} \end{aligned}$$

After segmentation an area threshold of 0.25 arcmin^2 was applied to discard unwanted regions. Subsequently, morph closing (a mathematical morphology operation consisting of dilation followed by erosion; Sonka et al. 2014) was applied with a 3 × 3 (cross) structuring function to get rid of the fragmentation in structures of interest (Figures 2(e)–(f)).

2.3. Plage Index Calculation

The plage index is an established metric, reflecting the occurrence of plage regions in Ca II K images. Following the description of plage index calculation in Bertello et al. (2010), from the mean normalized intensity histogram of the solar disc

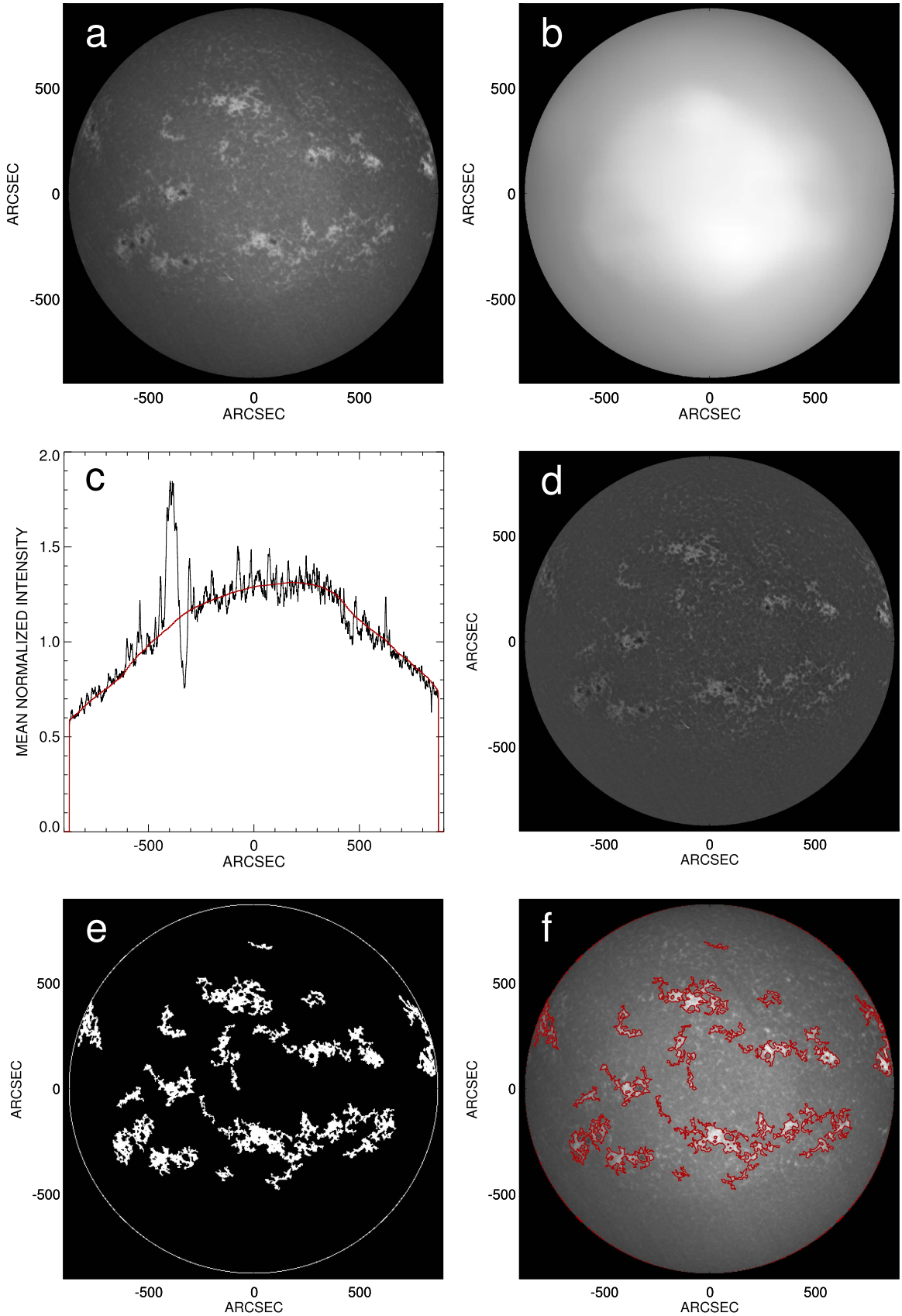

Figure 2. Processing steps involved for a representative KSO Ca II K image to detect plages. (a) Ca II K disc centered image. (b) Blurred image applying large window median filtering on (a) to understand the center-to-limb intensity variation. (c) *x*-profile overplotted through the center of (a) and (b). (d) Limb darkening corrected image. (e) Plage segmented image through row-wise thresholding. (f) Plage contour overplotted on (a).

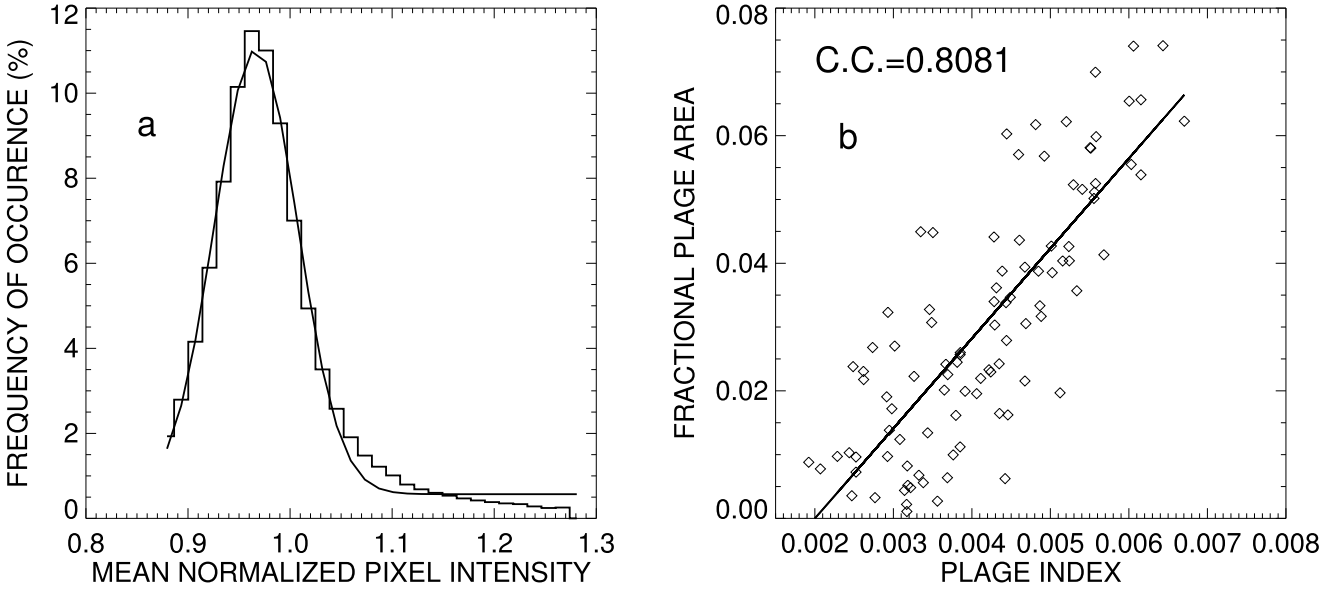

Figure 3. Validation of the current detection strategy. (a) Intensity histogram of a Ca II K image disc region and its Gaussian fit. (b) The correlation of the fractional plage area and the plage index with a least square linear fit is given by, Fractional Plage Area $= -2.82 \times 10^{-2} + 14.1133 \times$ Plage Index.

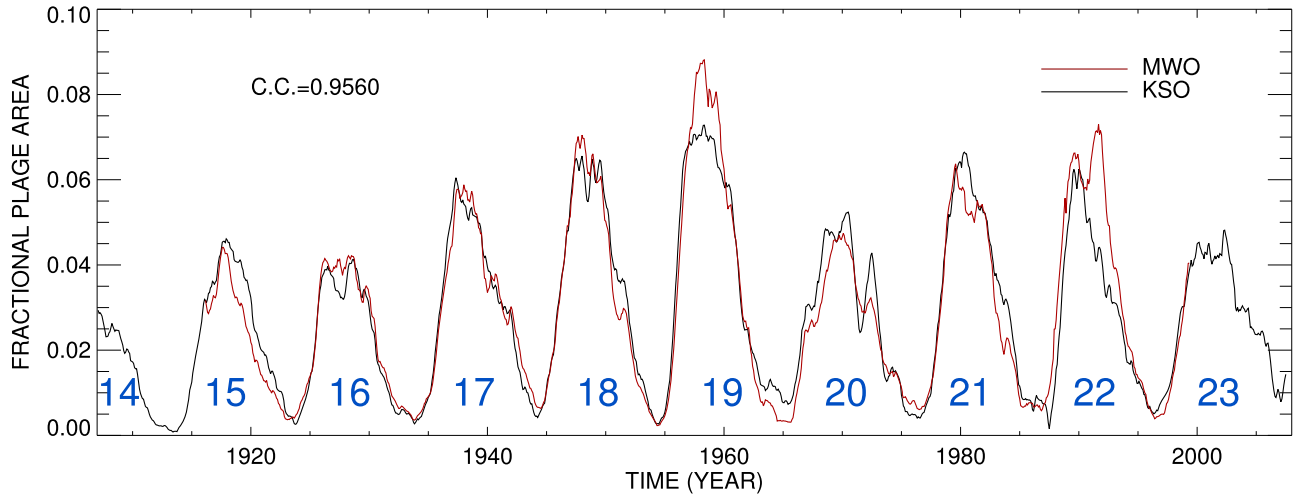

Figure 4. Ca II K plage area cycle depicting 12 months running average applied over the monthly average plage area. The black curve corresponds to the KSO Ca II K archival data and the red curve corresponds to MWO data. The least square linear fit for the overlapping region (1915–2000) is given by, $\text{Plage Fraction}_{\text{MWO}} = -0.0009 + 1.0252 \times \text{Plage Fraction}_{\text{KSO}}$. Cycle numbers are marked in blue.

with a bin width of 0.01, 35 bins were selected above and below the mode. Within this range a Gaussian was fitted to calculate the mean (μ) and variance (σ). Within $\mu - 2\sigma$ and $\mu + 7\sigma$, 30 bins were selected and another Gaussian ($f(x) = ke^{-\frac{(x-A)^2}{B}} + C$ where $(\mu - 2\sigma) \leqslant x \leqslant (\mu + 7\sigma)$) was fitted to it (Figure 3(a)). The constant term (C) of the Gaussian is called the plage index and indicates the asymmetry in the histogram wings due to the occurrence of high intensity regions called plages. For further validation, the correlation of the plage index with the fractional plage area acquired from plage detection is also presented (Figure 3(b)). Hereafter for solar cycle variation studies we will use the fractional plage area, the fraction of solar disc area covered by plages, as the most favorable proxy. The 12 month running average smoothing was performed on monthly averaged plage area cycles and is compared with the same for MWO in Figure 4.

2.4. Plage Centroid Detection and Butterfly diagram

After performing a morph closing operation on the binary plage detected images, individual connected structures were identified through giving certain labels to the pixels falling in the same region. Subsequently, centroid latitudes for all these regions were calculated for each image and were stacked over time to generate a butterfly diagram with four area thresholds for the plage regions 1 arcmin^2, 4 arcmin^2, 7 arcmin^2 and 10 arcmin^2 (Figure 6).

2.5. Carrington Map Generation

The Carrington map is a Mercator projection of the spherical Sun, mostly generated from daily observation for one solar rotation. In this study, 60° longitude bands (−30° to +30° heliographic longitude) on the limb darkening corrected full

disc Ca II K images were selected B_0 angle corrected, and stretched in the form of a rectangle with a weight of the fourth power of the cosine (Harvey & Worden 1998; Sheeley et al. 2011) over each longitude with respect to the central meridian. These slices were shifted and added according to the date and time for 27.2753 days to generate a full 360° map of the Sun. A similar 360° map, called a streak map, was obtained from rectangular binary slices (Sheeley et al. 2011). The overlaps of the same Carrington longitudes were removed through division of the original 360° map with a streak map to form an image called the Carrington map or synoptic map (Figures 5(a)–(d)). Carrington maps were also generated from a few Michelson Doppler Imager (MDI, on the *Solar Heliospheric Observatory*, *SOHO*) LOS full disc magnetograms available after 1996. Binary Carrington maps were generated for Ca II K and MDI using mean + σ and mean ± σ thresholds, respectively. These maps were further blurred using a Gaussian filter to account for the feature boundary uncertainty, and were cross-correlated for different relative x–y shifts.

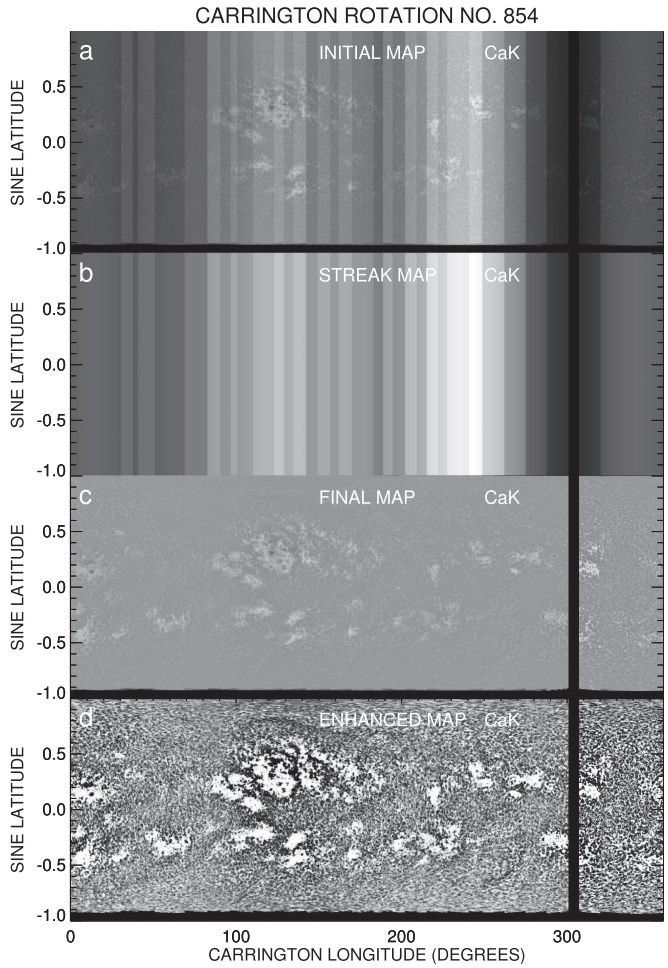

Figure 5. Carrington maps generated from KSO Ca II K full disc spectroheliograms starting on 1917 July 23. (a) Carrington map before overlap correction. (b) Streak map to determine overlaps. (c) Corrected map by division of (a) by (b). (d) Intensity enhanced map through histogram equalization.

3. RESULTS

For the study of the century-long magnetic activity of the Sun, Ca II K plage structures (Figure 2) with projected area $\geqslant$1 arcmin^2 have been used as the primary building block for a magnetic proxy. Their segmentation required an area threshold of 0.25 arcmin^2 to minimize the loss of fragmented plage structures before the morphological closing operation. This enabled us to deal with a good number of plage structures and to achieve desired statistics for the study of solar cycle variation. Histogram equalization on individual limb darkening corrected solar images resulted in uniformity in image contrast. This has also allowed us to detect the features automatically without any human bias of selection by visual inspection.

The area cycle, a temporal evolution of fractional disc area covered by plages, showed a good correlation (95.6%) with the same from MWO for the overlapping time period (Figure 4). This is an improvement over the earlier report by Priyal et al. (2014b) on KSO Ca II K data for the period 1955–1985, in which the correlation was shown to be 89%. It further revealed cycle 19 to be strongest one (Figure 4) and evidenced the double peak behavior in some of the cycles. Some unreal spikes were also observed at the cycle minima after 1975 due to the lower availability and the inferior quality of images. This was correlated with the occurrence of outlier points in the

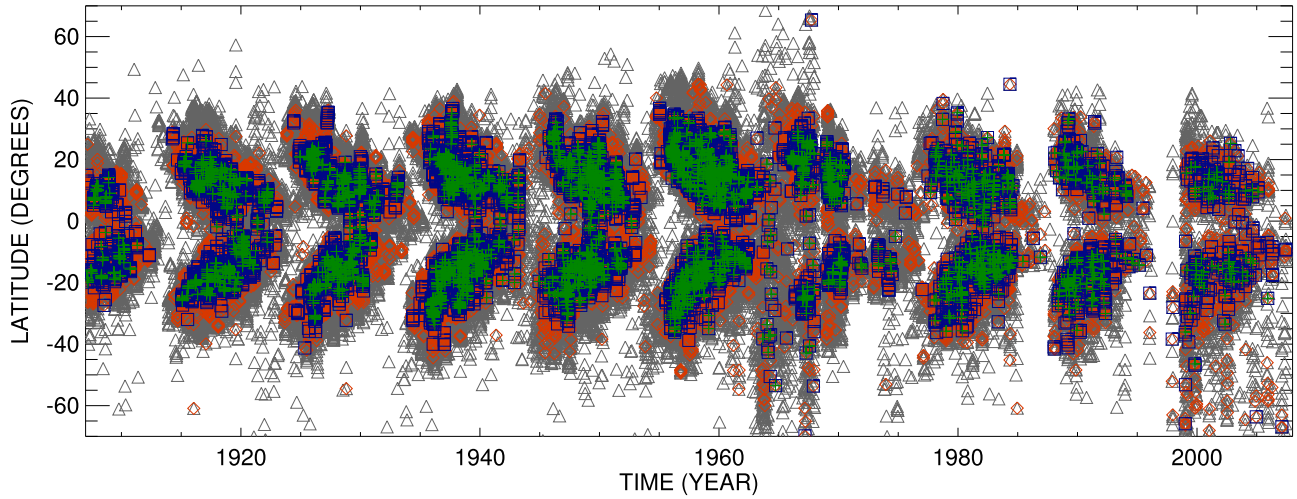

Figure 6. Ca II K butterfly diagram. Gray triangles depict centroids of plages with area $\geqslant$1 arcmin^2. The red, blue, and green symbols depict the centroids of plages with area $\geqslant$4 arcmin^2, $\geqslant$7 arcmin^2, and $\geqslant$10 arcmin^2 respectively.

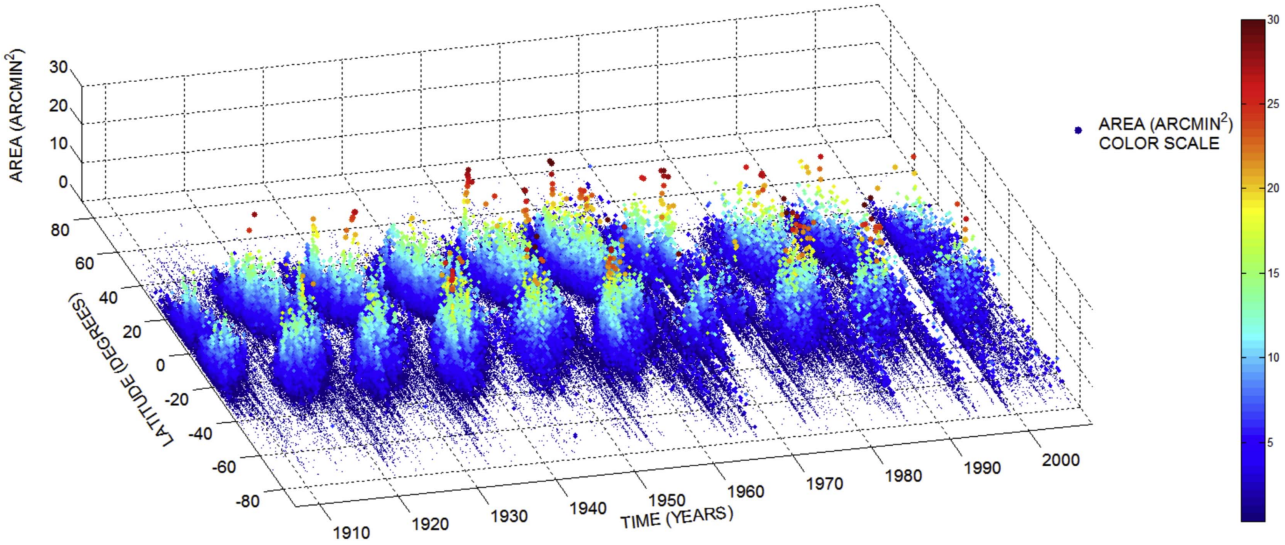

Figure 7. 3D visualization of the butterfly diagram with the area of the individual plages as the z-axis. The minimum to maximum plage area range is defined by dark blue to dark red through green, yellow, and orange, as indicated by the color scale.

(An animation of this figure is available.)

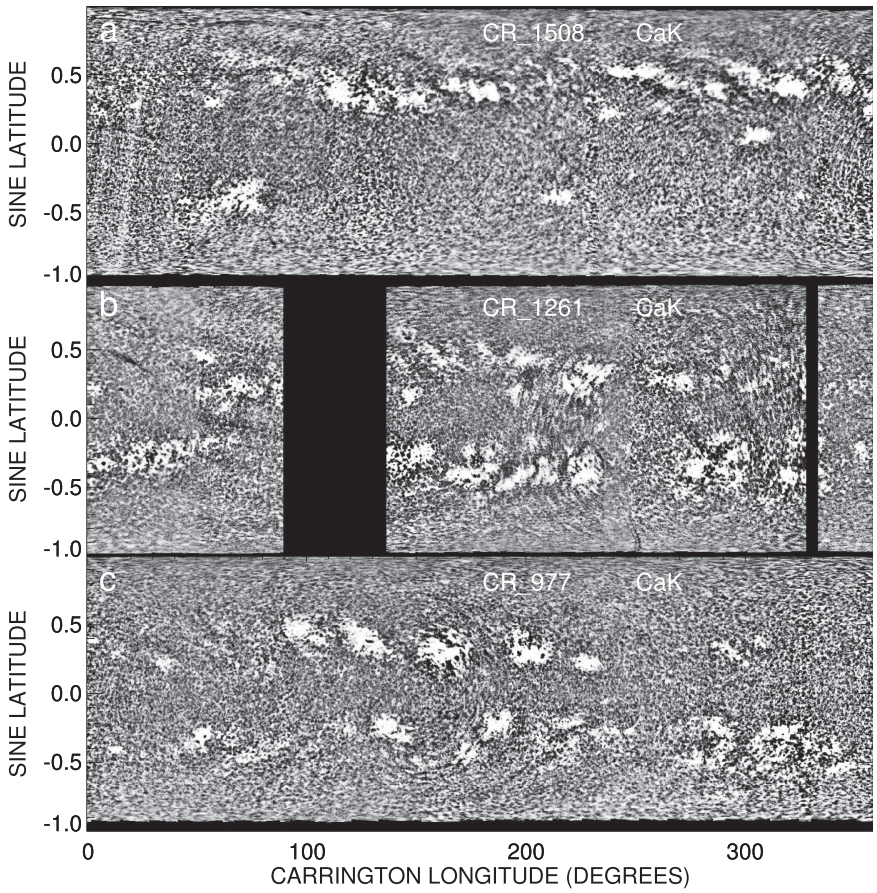

Figure 8. Carrington maps generated from KSO Ca II K full disc spectroheliograms. (a) Carrington map starting on 1966 May 25. (b) Carrington map starting on 1947 December 14. (c) Carrington map starting on 1926 September 29.

(An animation of this figure is available.)

butterfly diagram for some study period after 1985 (≈2 years) and 1994 (≈1 year). Those data points were removed using a criterion involving the maximum latitude of plage appearance at a certain phase of a cycle.

To explore the change in latitudinal distribution of enhanced Ca II K emission with time, we have produced the butterfly diagram. The centroids of plages have been used for the generation of this diagram, in contrast to Sheeley et al. (2011)

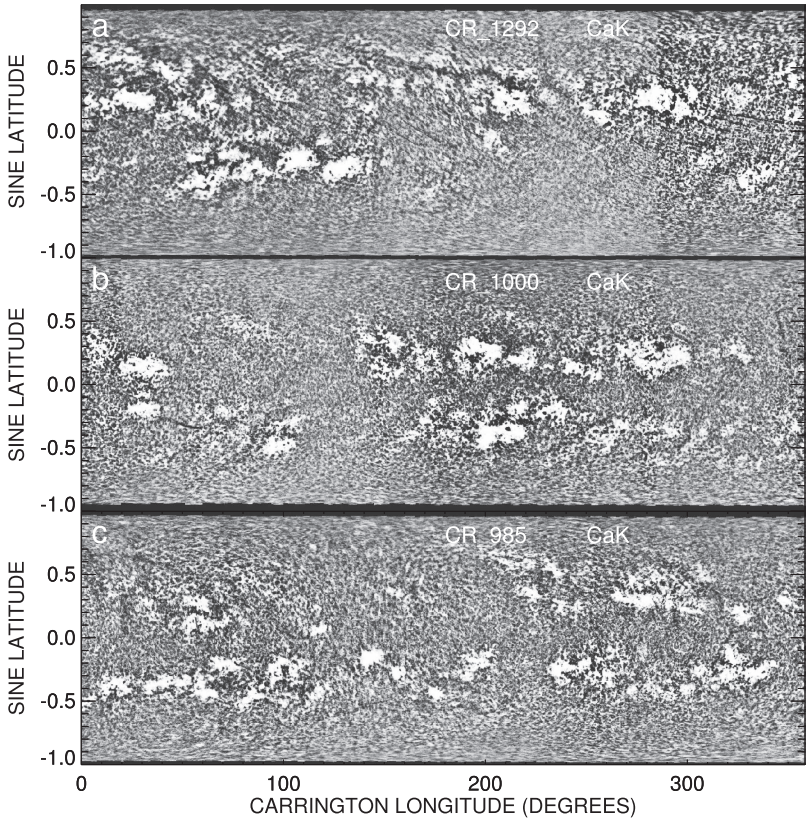

Figure 9. Carrington maps generated from KSO observatory Ca II K full disc spectroheliograms. (a) Carrington map starting on 1950 April 8. (b) Carrington map starting on 1928 June 17. (c) Carrington map starting on 1927 May 5.

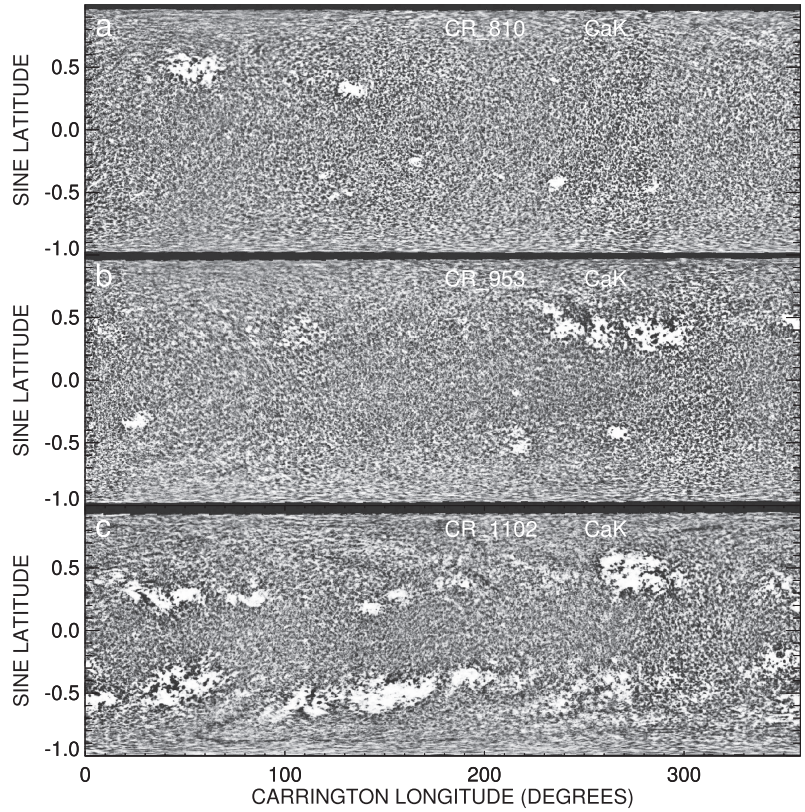

Figure 10. Carrington maps generated from KSO observatory Ca II K full disc spectroheliograms. (a) Carrington map starting on 1914 April 10, which is at the minimum phase between cycle 14 and 15. (b) Carrington map starting on 1924 December 13, which is at the minimum phase between cycle 15 and 16. (c) Carrington map starting on 1936 January 30, which is at the beginning of rising phase of cycle 17. For all these three maps the plages are mostly at higher latitudes $\approx 30°$.

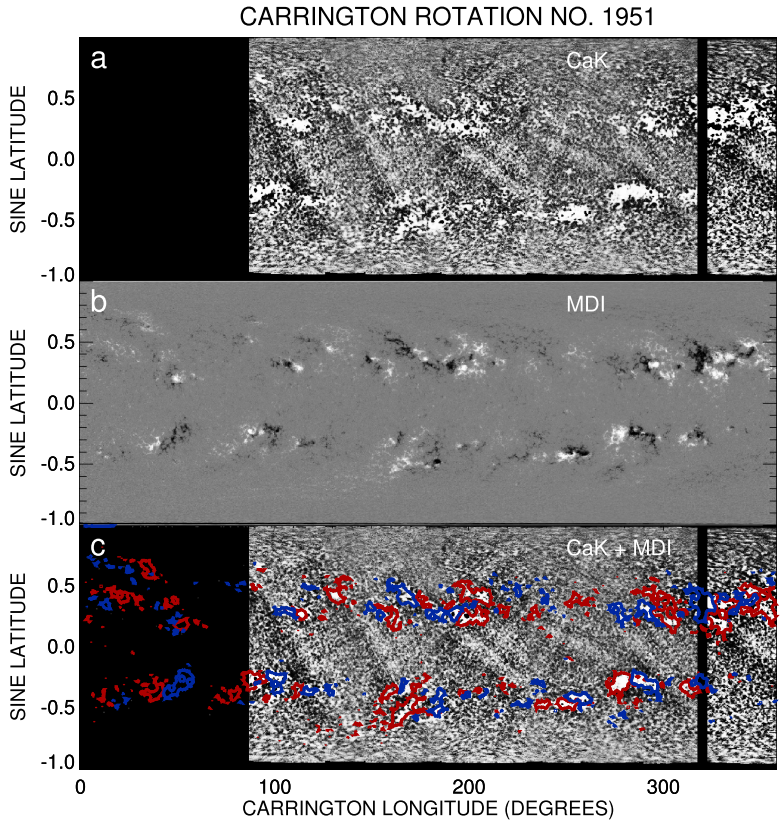

Figure 11. Overlap of plage structures and magnetic patches for CR, 1951. (a) Carrington map starting on 1999 June 24 generated from KSO Ca II K full disc spectroheliograms. (b) Carrington map generated from MDI full disc LOS magnetograms for the same rotation as that for Ca II K. (c) Contours of the large magnetic patches overplotted on (a). Red and blue depict toward and opposite to the LOS direction, respectively. Positional correlation ≈86.3%.

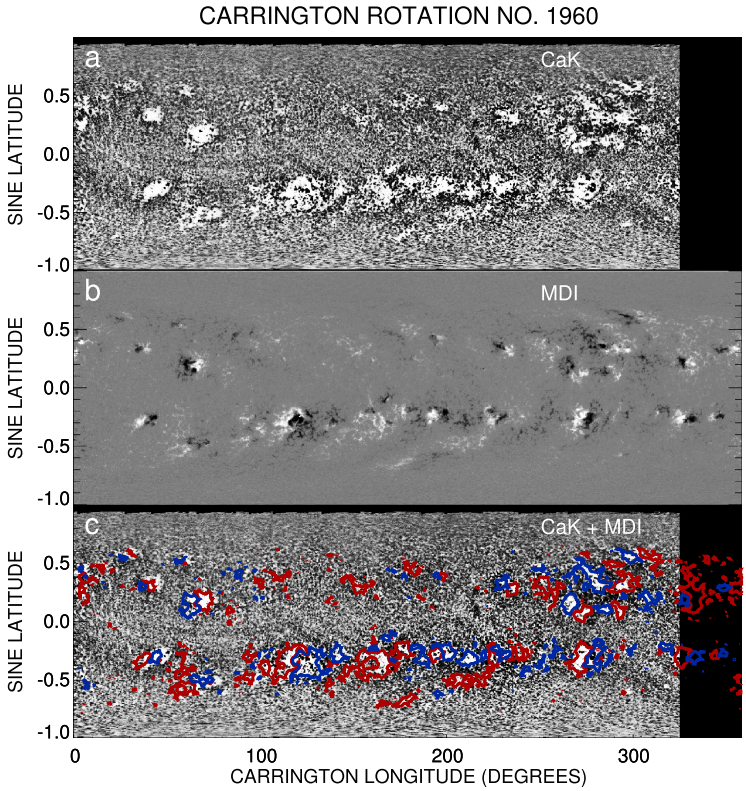

Figure 12. Overlap of plage structures and magnetic patches for CR, 1960. (a) Carrington map starting on 2000 February 25 generated from KSO Ca II K full disc spectroheliograms. (b) Carrington map generated from MDI full disc LOS magnetograms for the same rotation as that for Ca II K. (c) Contours of the large magnetic patches overplotted on (a). Red and blue depict toward and opposite to the LOS direction, respectively. Positional correlation ≈85.5%.

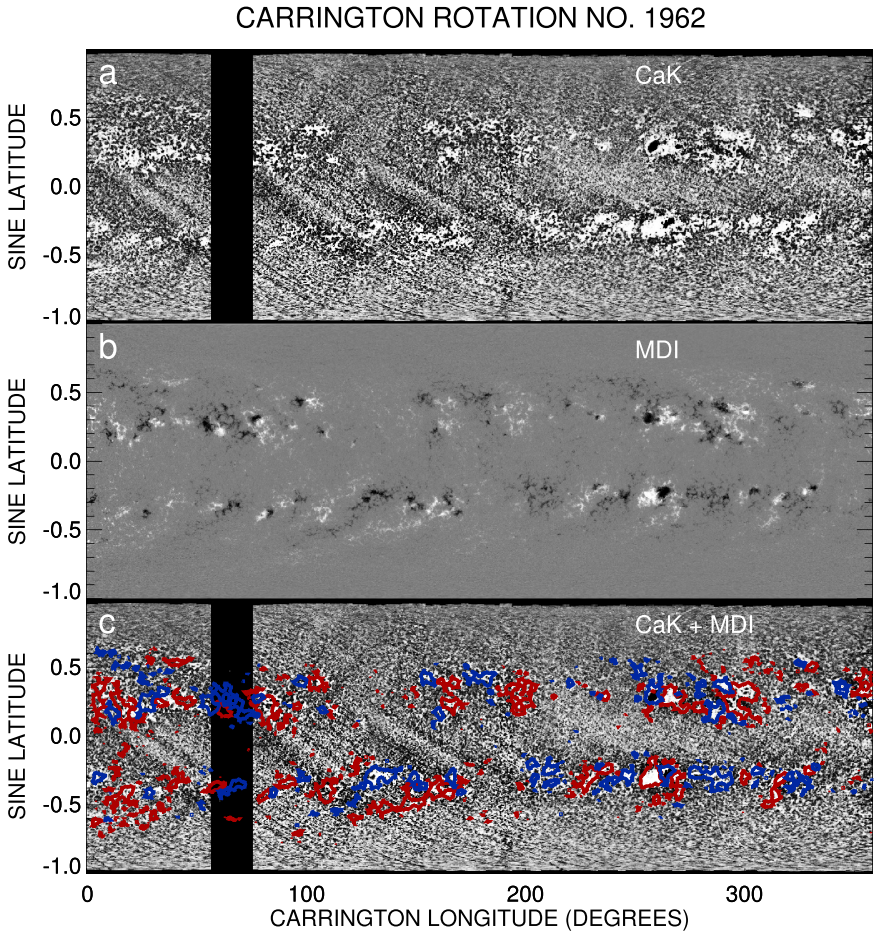

Figure 13. Overlap of plage structures and magnetic patches for CR, 1962. (a) Carrington map starting on 2000 April 19 generated from KSO Ca II K full disc spectroheliograms. (b) Carrington map generated from MDI full disc LOS magnetograms for the same rotation as that for Ca II K. (c) Contours of the large magnetic patches overplotted on (a). Red and blue depict toward and opposite to the LOS direction, respectively. Positional correlation ≈75.1%.

who used the Carrington maps for the same. The butterfly diagram with three area thresholds (Figure 6) reveals that higher plage areas are more concentrated at the equator with a spatial correlation with active regions (Stix 2004). In order to obtain a better visualization of the latitudinal variation of different sizes with time, a 3D version of the butterfly diagram was created, adding the individual projected plage areas as the third dimension (Figure 7). An animated figure has also been created to demonstrate how the time–latitude distribution changes with variation of plage size. This dynamic illustration is available online and can also be found at ftp://ftp.iiap.res.in/subhamoy/cak_carrington_maps_kodaikanal/butterfly_cak_3d.gif. Figures 6 and 7 can be readily compared with well known butterfly diagrams as generated from sunspot areas, showing higher-latitude to equatorward occurrence of plage structures for each cycle. It should be noted that due to the area thresholding the smallest features, like network bright points, are not detected in the current analysis and the poleward migration is not observed (Priyal et al. 2014a).

It was pointed out earlier that the enhanced emission in Ca II K relates well to the magnetic field concentrations. Thus the Carrington maps indicate the magnetic flux distribution over a solar rotation. In this article we presented synoptic or Carrington maps (Figures 8(a)–(c)) incorporating plage evolutions for different solar rotations over the past 100 years. These maps will be particularly useful for the period for which LOS magnetograms are not available. Similar maps were generated by Sheeley et al. (2011) from MWO Ca II K data. First we will compare a few representative cases of newly generated Carrington maps from KSO data and those of MWO. Figures 8(a), (b), and (c) can be compared with the upper panel of Figure 4, the lower panel of Figure 7, and the lower panel of Figure 10 of Sheeley et al. (2011), respectively. The close resemblance of these maps provides a good validation of calibration and map generation, and portray the quality of the KSO data. The longitude band selected for each full disc image to generate the map was the result of a trade off between feature sharpness and data gap (Figure 8(b)). However, apart from geometrical similarity, a difference in the contrast and visibility of network structures can be observed between the maps from KSO and MWO. This might have occurred because of the difference in digitization and preprocessing of the full disc images. In Figures 9(a)–(c) and 10(a)–(c) we show a few more examples of CR maps corresponding to different phases of the solar cycle as generated from KSO spectroheliograms without any data gaps. Enhanced Ca II K Carrington maps at later times (after 1990) show bright tilted periodic artefacts because of a higher occurrence of scratches in the spectroheliograms.

Next we compare our Ca II K Carrington maps to Carrington maps of photospheric magnetic fields generated from full disc LOS magnetograms of MDI on *SOHO*. Cross-correlation of all sample Carrington maps from Ca II K (KSO) and MDI show a maximum

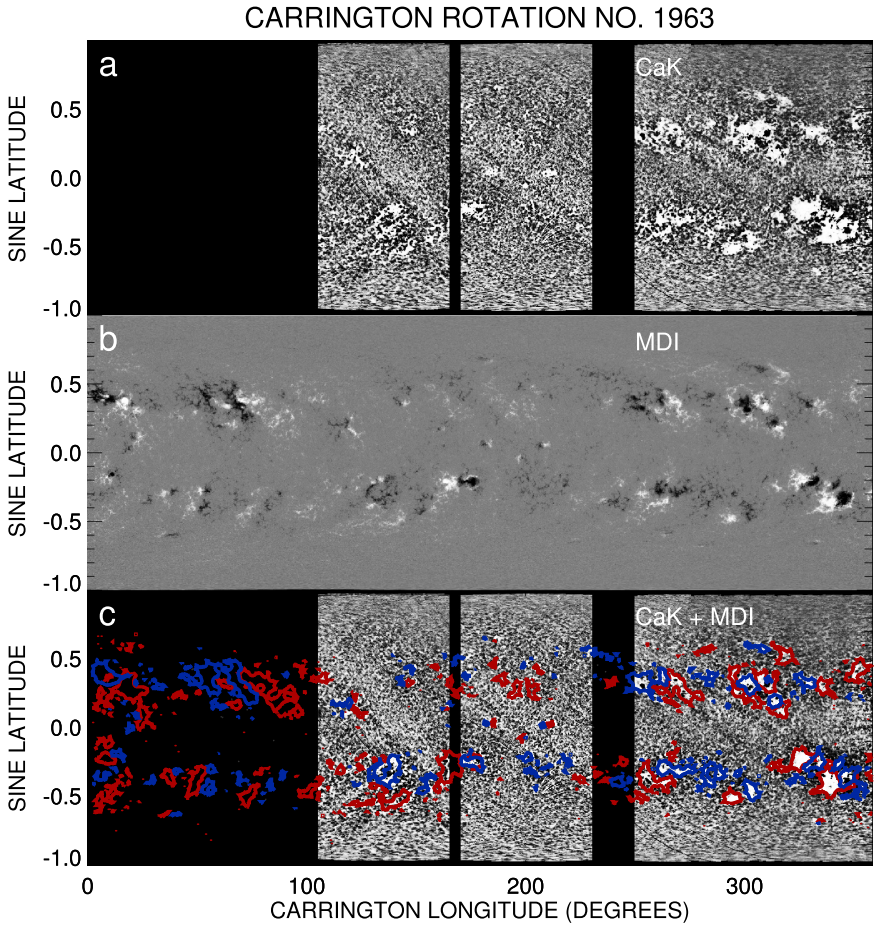

Figure 14. Overlap of plage structures and magnetic patches for CR, 1963. (a) Carrington map starting on 2000 May 17 generated from KSO Ca II K full disc spectroheliograms. (b) Carrington map generated from MDI full disc LOS magnetograms for the same rotation as that for Ca II K. (c) Contours of the large magnetic patches overplotted on (a). Red and blue depict toward and opposite to the LOS direction. Positional correlation ≈92.3%.

overlap at a relative *x*-shift and *y*-shift of about 5 pixels and 9 pixels, respectively, where the size of the maps was 1571 × 500. This study reveals good spatial correlation (⩾75%) between the magnetic patches and plage structures (Figures 11–14). Carrington maps from 1907 to mid-2007 have been provided as supplementary material (also available at ftp://ftp.iiap.res.in/subhamoy/cak_carrington_maps_kodaikanal/). We also provide a time lapsed movie which includes all the maps for the period of 100 years, see Figure 8 (also available at ftp://ftp.iiap.res.in/subhamoy/cak_carrington_maps_kodaikanal/cak_video_1907_2007.gif).

4. CONCLUSION

We have used Ca II K line images, recorded by KSO, digitized and calibrated by our group, to construct Carrington maps and butterfly diagrams corresponding to the period of 1907–2007. The KSO data allow us to study the cyclic activity of the solar magnetic fields for a longer time-span (>100 yr) in contrast to that from MWO, which covers about 85 yr (Bertello et al. 2010). Sheeley et al. (2011) studied Carrington maps from 1915–1985 from the MWO archive, whereas the current study generated Carrington maps from 1907 to mid-2007 using images which were recorded at the KSO. These maps provide ways of tracking magnetic field distributions all the way back to 1907, a period for which direct magnetic field synoptic observations are not available. In the context of the long term evolution of features on the Sun at specific wavelengths, the present study segmented the plage structures, and generated area cycle and butterfly diagrams from the 100 yr Ca II K KSO data. The derived century-long Ca II K synoptic maps further elaborated on the correlation with the same generated from space-based magnetograms for an overlapping study period and confirmed their physical connection (Stix 2004; Sheeley et al. 2011).

Figure 7 illustrates the cyclic behavior of the projected area for individual plages at different latitude bands. It also gives a hint about the relative delay in attaining the cycle peak for individual plage area between different latitudes. Thus this area-scaled butterfly diagram provides some additional information for a greater time-span (1907–2007), in contrast to the super synoptic map presented in Sheeley et al. (2011) with a study period between 1915 and 1985. The location pf overlap between the plage structures and magnetic patches in turn validated the theoretical expectation of a higher field strength being correlated with less Ca II K absorption (Pevtsov et al. 2016). Therefore, the century-long Ca II K data can act as a proxy for understanding the locational evolution of magnetic patches.

This study demonstrated the importance of the century-long Ca II K spectroheliograms in delineating evolutionary features from different perspectives and determining their possible correspondence. Observations on the latitude-dependent plage

area variation can provide more insight for the conventional area cycle, as it is an aggregate. Along with the study of long term evolution, some smaller timescale phenomena can also be analyzed from this huge data set. The rotation rate variation for different latitudes can be analyzed from plage areas over a period of 100 yr (Singh & Prabhu 1985; Kiepenheuer 2012). Machine learning techniques can be applied on and validated through this huge data set, providing confidence for the prediction for future cycle characteristics (Colak & Qahwaji 2009). We propose to address some of these aspects in future studies.

We hope that the results presented here and the Carrington maps published online (ftp://ftp.iiap.res.in/subhamoy/cak_carrington_maps_kodaikanal/) will also help the global community to study different features at a greater depth, and in this the new database available at https://kso.iiap.res.in/data will act as a valuable resource. Recently Pevtsov et al. (2016) have attempted to create a homogeneous, long term series of pseudo-magnetograms using a combination of Ca II K line images and sunspot polarity measurements. We hope to pursue the same in the near future for our KSO data. We further propose combining the MWO and KSO data sets to produce a single improved set. This will also enable us to fill the data gaps in the two independent data sets. This cross-calibration and comparison will yield a data series with uniform quality. We would like to mention that further refinements, improvements in the calibration process, and cross-calibration between different data series will be released from time to time through our web portal at https://kso.iiap.res.in/data with marked versions and data products.

We would like to thank all the observers at KSO over 100 years for their contribution to building this enormous resource. The current high resolution digitization process was initiated by Prof. Jagdev Singh and we thank him for his substantial contribution to the project. We would like to thank many who have helped in the digitization and calibration: Muthu Priyal, Amareswari, T. G. Priya, Ayesha Banu, A. Nazia, S. Kamesh, P. Manikantan, Janani, Manjunath Hegde, Trupti Patil, Sudha, and staff members at KSO who also helped us in setting up the digitizer unit and the digitization at KSO. We also thank the anonymous referee, whose valuable comments helped us to improve the presentation.

REFERENCES

Bertello, L., Ulrich, R. K., & Boyden, J. E. 2010, SoPh, 264, 31
Colak, T., & Qahwaji, R. 2009, SpWea, 7, s06001
Ermolli, I., Solanki, S. K., Tlatov, A. G., et al. 2009, ApJ, 698, 1000
Foukal, P., Bertello, L., Livingston, W. C., et al. 2009, SoPh, 255, 229
Foukal, P., & Lean, J. 1988, ApJ, 328, 347
Harvey, J., & Worden, J. 1998, in ASP Conf. Ser. 140, Synoptic Solar Physics, ed. K. S. Balasubramaniam, J. Harvey, & D. Rabin (San Francisco, CA: ASP), 155
Jin, C., & Wang, J. 2015, ApJ, 806, 174
Kiepenheuer, K. 1968, in IAU Symp., Structure and Development of Solar Active Regions, ed. K. O. Kiepenheuer (Netherlands: Springer), 35
Pevtsov, A. A., Virtanen, I., Mursula, K., Tlatov, A., & Bertello, L. 2016, A&A, 585, A40
Priyal, M., Banerjee, D., Karak, B. B., et al. 2014a, ApJL, 793, L4
Priyal, M., Singh, J., Ravindra, B., Priya, T. G., & Amareswari, K. 2014b, SoPh, 289, 137
Schrijver, C. J., Cote, J., Zwaan, C., & Saar, S. H. 1989, ApJ, 337, 964
Sheeley, N. R., Jr., Cooper, T. J., & Anderson, J. R. L. 2011, ApJ, 730, 51
Singh, J., & Prabhu, T. 1985, SoPh, 97, 203
Skumanich, A., Smythe, C., & Frazier, E. N. 1975, ApJ, 200, 747
Sonka, M., Hlavac, V., & Boyle, R. 2015, Image Processing, Analysis, and Machine Vision (Andover: Cengage Learning)
Stix, M. 2004, The Sun: An Introduction (Berlin: Springer)
Zharkova, V., Ipson, S., Benkhalil, A., & Zharkov, S. 2005, Artif. Intell. Rev., 23, 209